SCIENCE CHINA
Chemistry

• REVIEWS •
• SPECIAL ISSUE • In Honor of the 80th Birthday of Professor WANG Fosong

May 2012 Vol.55 No.5: 726–734
doi: 10.1007/s11426-012-4501-5

Polystyrene-based blend nanorods with gradient composition distribution

WU Hui[1], SU ZhaoHui[2], TERAYAMA Yuki[3] & TAKAHARA Atsushi[1,3*]

[1]*Institute for Materials Chemistry and Engineering, Kyushu University, Fukuoka 819-0395, Japan*
[2]*State Key Laboratory of Polymer Physics and Chemistry, Changchun Institute of Applied Chemistry, Chinese Academy of Sciences, Changchun 130022, China*
[3]*Graduate School of Engineering, Kyushu University, Fukuoka 819-0395, Japan*

Received October 3, 2011; accepted November 20, 2011; published online February 17, 2012

The polystyrene-based polymer blends, partially miscible poly(bisphenol A carbonate)/polystyrene (PC/PS) and completely miscible poly(2,6-dimethylphenylene oxide)/polystyrene (PPO/PS), in nanorods with gradient composition distribution were discussed. The polymer blend nanorods were prepared by infiltrating the polymer blends into nanopores of anodic aluminum oxide (AAO) templates via capillary action. Their morphology was investigated by micro-Fourier transform infrared spectroscopy (micro-FTIR) and nano-thermal analysis (nano-TA) with spatial resolution. The composition gradient of polymer blends in the nanopores is governed by the difference of viscosity and miscibility between the two polymers in the blends and the pore diameter. The capillary wetting of porous AAO templates by polymer blends offers a unique method to fabricate functional nanostructured materials with gradient composition distribution for the potential application to nanodevices.

nanorods, gradient composition distribution, polymer blends, anodic aluminum oxide, micro-FTIR, nano-TA

1 Introduction

One-dimensional (1-D) polymeric nanomaterials have attracted increasing interest due to their unique properties and potential applications in many areas, such as electronics, mechanical, optical, sensor and biomedical devices [1, 2]. Different strategies have been carried out to generate well-defined 1-D nanostructures with high aspect ratios (length/diameter), such as template infiltration [1–31], self-assembly of microphase-separated block copolymers [32–37], electrospinning [38–42], and nanoimprint lithography (NIL) [43–45]. Among those developed approaches, one of the most promising methods is the use of templates to prepare the 1-D nanomaterials.

Generally, two types of nanoporous templates, track-etch polymeric membrane and inorganic anodic aluminum oxide (AAO) membrane, are commonly used to fabricate 1-D polymer nanomaterials [1]. Especially for the self-ordered AAO membrane, because of the aligned, rigid, and separated cylindrical nanopores, it is an ideal template for the preparation of polymer nanomaterials with monodisperse diameters ranging from nanoscale to microscale. The feature size and shape of the fabricated nanomaterials can be easily controlled by the distribution of template pores. Via an electrochemical anodization process, the AAO templates with pore sizes ranging from about 5 nm up to a few hundred nm [1] and pore depths from several nm to several hundred μm are obtainable. The thermal stability and mechanical rigidity of the inorganic alumina wall provide a strictly 2-D constrained environment and avoid breakdown of the cylindrical confinement. Thus, this highly versatile template allows fabricating 1-D polymeric nanomaterials including polymer nanotubes, nanowires and nanorods, by template synthesis [1], melt-wetting [3–24], solution-wetting [24–28],

*Corresponding author (email: takahara@cstf.kyushu-u.ac.jp)

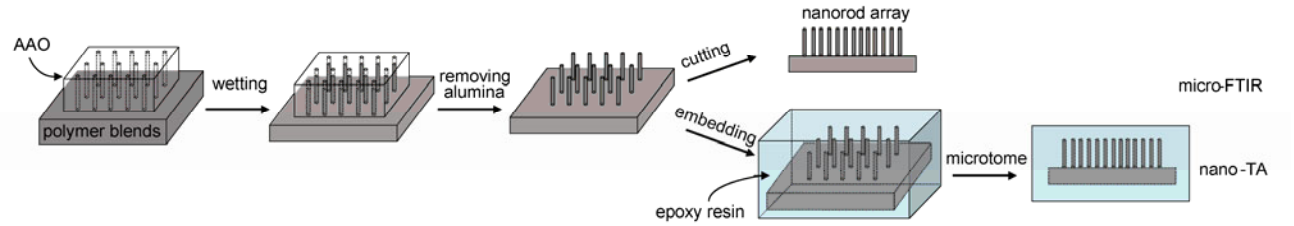

Figure 1 Schematic of sample preparation for micro-FTIR and nano-TA measurement.

vacuum filtration [29], and melt compression [30, 31].

For nanomaterials, their internal morphology largely determines their mechanical, optical, and electrical properties. Hence, much effort is devoted to precisely control the spatial and anisotropic order for the 1-D polymer nanostructures, by which they offer diverse and versatile benefits as they are good subjects for experimental [1–31] and simulation [46–51] studies on behavior and properties of polymer nanomaterials. A number of techniques, such as transmission electron microscopy (TEM) [3–6], differential scanning calorimetry (DSC) [7–9], Fourier transform infrared (FTIR) [10], X-ray diffraction (XRD) [9, 12, 35], dielectric spectroscopy [15, 16], and small-angle neutron scattering (SANS) [17, 18], have been applied to study the polymers in cylindrical nanopores. The 1-D nanostructures with novel phase morphology [3–6], enhanced mobility [17], unusual crystallization process [7–9], specific crystal orientation [9–16, 25], chain dynamic behavior [15–19], and polymorphic behavior [20] have been demonstrated.

When the amorphous phase-separating block copolymers are developed in cylindrical nanopores, due to interactions between polymer blocks and pore walls, commensurability between pore diameter and the natural period of block copolymers (BCPs) morphology in the bulk, and the curvature that is forced on the BCPs morphology, the BCPs can break the bulk balance and self-assemble into a variety of unprecedented structures, such as concentric lamellae, core shell cylinders, stacked disks, torus-like morphologies, and helical morphologies [3–6]. In the case of amorphous polystyrene (PS) confined in cylindrical alumina nanopores, an unexpected enhancement of flow and a reduction in intermolecular entanglement occurs, causing higher mobility of polymer in the confined geometry than that of unconfined chains [17].

For the semi-crystalline polymers under nanocylindrical geometry, the finite size of the domains affects the crystallization process drastically. A transformation from a predominantly heterogeneous to predominantly homogeneous nucleation takes place if the pore diameter is smaller than 65 nm. Crystallization is suppressed with decreasing pore size, and is completely stopped in pores below 20 nm diameters [8]. The orientation of crystals in the nanocylinders is strongly dependent on the crystallization temperature. The crystals crystallized at high supercooling have no preferred orientation [10, 35]; while the crystals crystallized at low supercooling show perpendicular orientation, that is, the *c*-axes of the polymer crystals preferentially orient perpendicular to the long axis of the nanorod [9–16, 25], which can be attributed to the selective crystal growth compatible with the nanocylindrical confinement [9, 35]. A mixture of crystalline phases can be produced in the nanorods and this polymorphic behavior can be explained as the different nucleation behavior occurs at different temperatures within the confinement of nanopores [20].

Blending of polymers is a flexible way, usually a more cost-effective way than in the case of synthesis of new polymers, to produce novel materials [52, 53]. The morphology and properties of polymer blends are largely determined by the microstructure of the system, which depends upon the interaction and miscibility of the components. According to the miscibility, the blends can be classified into three groups: immiscible, partially miscible and completely miscible blends. The glass transition temperature (T_g) measurement is frequently used to estimate the compatibility of blends. Immiscible polymer blends exhibit two glass transitions at temperatures around those of the components. Partially miscible systems are heterogeneous two-phase structure, in which only a limited amount of the other component is dissolved in both phases. Two T_gs in these polymer pairs approach each other but do not become identical. Completely miscible blends result in homogeneous structure and show a single T_g between the T_g of the individual components.

Based on readily available polymers, the unusual polymer blends with a combination of properties unattainable in any single polymer component are obtainable. For instance, the partially miscible polycarbonate/polystyrene (PC/PS) blends [54–56] exhibit excellent flame retardancy and high fluidity, critical for the development of environmentally friendly materials and thin wall applications for packaging of electronic goods. Completely miscible poly(2,6-dimethylphenylene oxide)/polystyrene (PPO/PS) blends having good dimensional stability, high resistance to moisture, impact resistance, low temperature impact strength, low creep, and good processability, are widely used in automotive instrument panels, interior trim, business equipment chassis, electrical applications, and medical equipment. Therefore, it is meaningful to develop polymer blend nanomaterials which could lead to functional nanodevices with unique and exciting properties for potential applications in nanotech-

nologies. Here, the preparation and morphology of polystyrene-based blends, both partially and completely miscible, in cylindrical nanopores with gradient composition distribution, are discussed.

2 Formation of polymer blend nanorods

Porous AAO templates were used to prepare the polymer blend nanorods. Figure 1 shows a schematic diagram of the process used to introduce the polymer blends into the cylindrical alumina pores. The self-ordered templates with diameter of 300, 65, and 35 nm and depth of 140 μm were fabricated via a two-step anodization process using phosphoric acid, oxalic acid and sulfuric acid as electrolyte, respectively [57, 58]. The SEM images of AAO templates with different diameters are shown in Figure 2. The templates consist of a hexagonal array of parallel cylindrical pores oriented perpendicularly to the surface of the template.

The polymer blend melts were drawn into the nanopores of the membrane via capillary action. Inorganic materials like AAO templates are considered as high surface energy materials with respect to their surface energies, whereas most polymer melts (e.g. PC, PPO and PS) are of lower surface energies. When placed the porous AAO templates on top of a 200 μm thick compression-molded PC/PS or PPO/PS blend film (PC: M_n = 24600, M_w/M_n = 1.88; PPO: M_n = 15500, M_w/M_n= 2.16; PS: M_n = 115000, M_w/M_n= 1.04) with weight ratio of 1:1, the low-energy polymer melts can wet the high-energy pore surfaces easily. After annealed polymer blend melts/AAO assembly for several hours under vacuum, the polymer blends enter nanopores by capillary force. When quenched to room temperature, the polymer blend melts within nanopores were solidified and the polymer nanostructures were generated. The resultant polymer blend nanorods can be released from AAO templates by selectively removing the alumina using phosphoric acid or sodium hydroxide aqueous solutions. Figure 3(a, b, c) show the representative SEM micrographs of parallel aligned PC/PS blend nanorods with diameters of 300, 65, and 35 nm. The nanorods protruding from the substrate blend film are shown in Figure 3(d). With the tips of the nanostructures being removed (Figure 3(e)), solid rod structure appeared in the center of generated nanomaterials [10].

3 Micro-FTIR analysis

The polymer compositions in blend nanorods/film can be analyzed by micro-FTIR because micro-FTIR provides a simple and powerful approach for local analysis to get high spatial resolved information with advantages of nondestructive and fast measurement. The microscope connected with a PerkinElmer FTIR (Spectrum One) includes a viewing system so that a point of interest in the sample can be observed, positioned, and measured. The optical image of the sample was displayed on the computer monitor, and the operation of the microscope, map and collect spectra from the sample was controlled by the Autoimage software.

Figure 4(A) shows a representative optical micrograph of a thin slice of a PC/PS nanorods/film prepared with an AAO template comprising of 300 nm diameter pores. The area on the top is the nanorod array standing on the bulk film after removal of AAO template, which appears darker due to the scattering of light at the numerous nanorod/air interfaces, while the translucent section on the bottom is the cross section of the residual PC/PS film [10]. To the right of Figure 4(A) depicts the schematic of nanorods connected with bulk film. During the measurement a spatial resolution of 300 × 30 μm^2 was employed and the resolution along the long axis of rod was 30 μm to obtain the spectra from the top to the bottom in the thin slice.

The corresponding micro-FTIR spectra of 300 nm diameter PC/PS nanorods in the measured position are shown in Figure 4(B). The top three curves are the spectra of nanorods in the position of a, b, and c, while the bottom three curves represent the residual bulk film in the position of d, e, and f, respectively. In the spectra, the relative intensity of PC bands at 1776 cm^{-1} (carbonyl stretching of carbonate

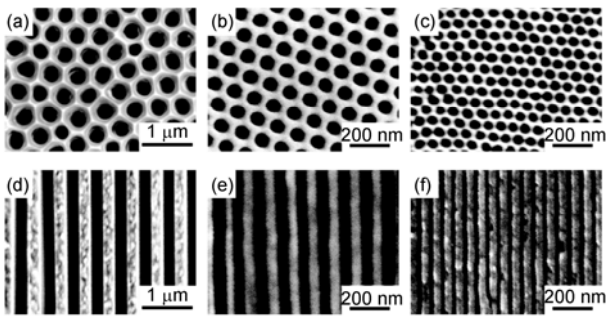

Figure 2 SEM micrographs of AAO templates with pore diameters of (a, d) 300 nm; (b, e) 65 nm; (c, f) 35 nm. (a, b, c) top view of the AAO templates; (d, e, f) cross section of the AAO templates.

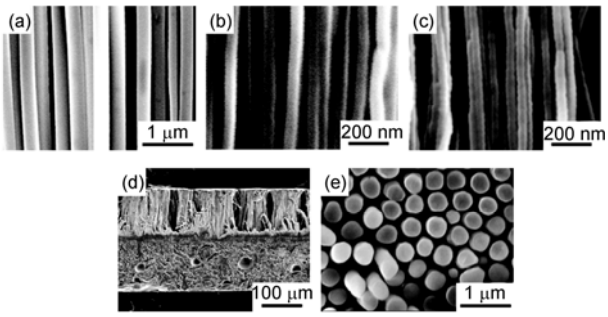

Figure 3 SEM micrographs of PC/PS nanorods prepared by infiltrating the AAO template with a PC/PS melt: (a, d, e) 300 nm; (b) 65 nm; (c) 35 nm. (a, b, c, d) cross section of the nanorod array; (e) top view of the nanorod array with the tips of the nanorods removed.

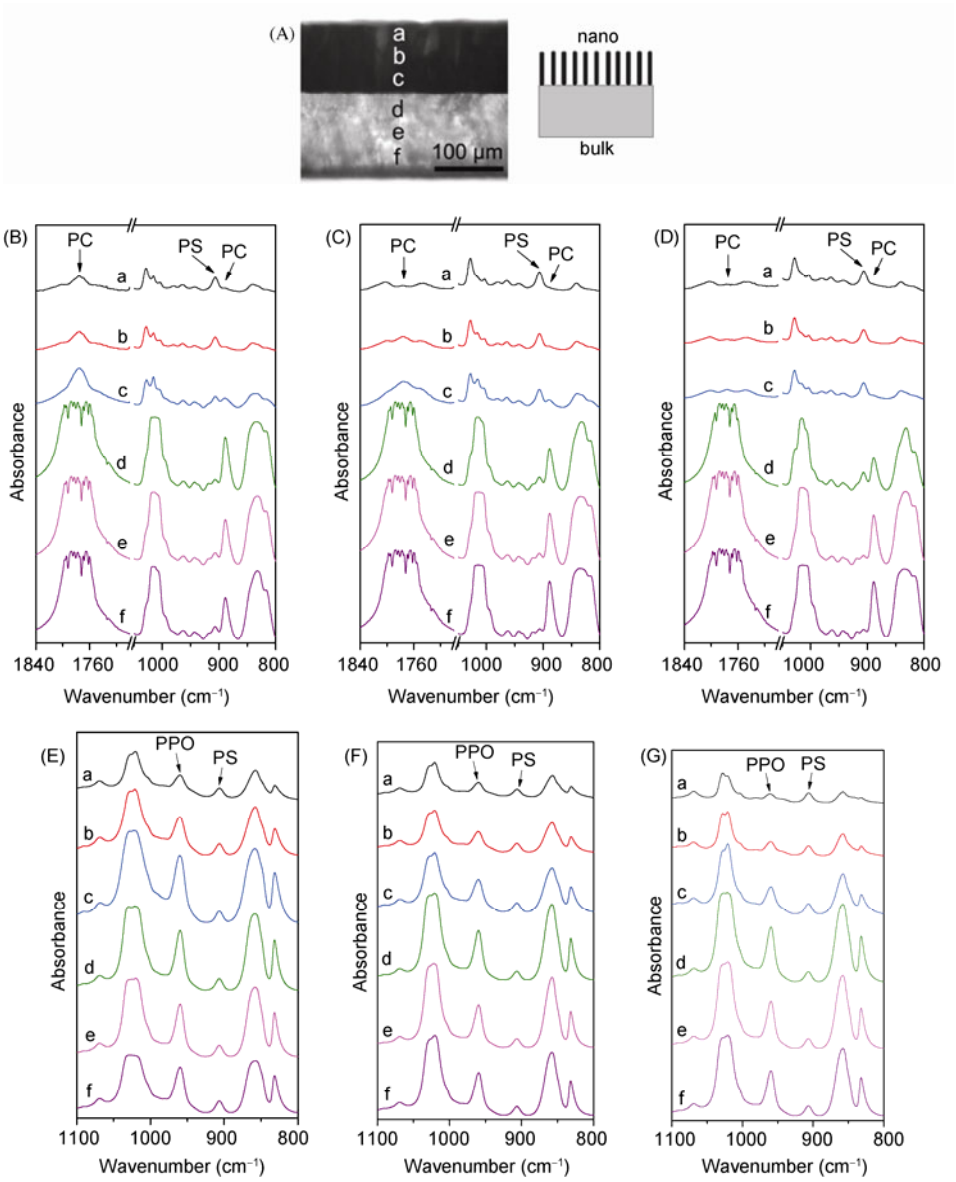

Figure 4 (A) Representative optical micrograph of a thin slice of a PC/PS nanorods/film prepared with an AAO template comprised of 300 nm diameter pores. The darker section on the top is the nanorod array. To the right is a schematic of nanorods connected with bulk film. The corresponding micro-FTIR spectra of PC/PS nanorods (modified from [22]. Copyright 2011 The Royal Society of Chemistry) with diameter of 300 nm (B), 65 nm (C), and 35 nm (D), and PPO/PS nanorods (modified from [23]. Copyright the Society of Polymer Science, Japan) with diameter of 300 nm (E), 65 nm (F), and 35 nm (G) at the measured positions, respectively.

functional group [59]) and 888 cm^{-1} (C–CH_3 stretching [59]) enhanced the position from a to c, indicating PC content in the nanorods increased from the top side to the bottom side and a composition gradient formed in the partially miscible polymer blend nanorods along the long axis of rod. And these similar results were also observed in the nanorods of 65 (Figure 4(C)) and 35 nm (Figure 4(D)), showing the same trend that a gradient composition distribution formed in smaller nanorods.

The PS content at different positions in the nanorods/film can be obtained by examining two specified bands at 906 cm^{-1} (out-of-plane vibration of benzene ring of PS [60]) and 888 cm^{-1} [22, 61]. A quantitative comparison of the PS content for both nanorods and the bulk at different positions extracted from the FTIR data is shown in Figure 5(A). Although the PS content in the original PC/PS bulk film was about 50%, the PS content in nanorods is much higher than that in bulk, reflecting the PS component preferentially occupied the nanopores. The PS content in all the nanorods of 300, 65 and 35 nm diameter decreased from the top (position a) to the bottom (position c). The PS content of 35 nm diameter nanorods in different positions was higher than that in the 65 and 300 nm diameters, showing the PS content in nanorods increased as the pore diameters became

smaller and the degree of confinement imposed by the nanopores greatly influences the composition distribution of polymer blends in nanorods.

The micro-FTIR spectra of completely miscible PPO/PS blends in nanorods of 300, 65, and 35 nm are shown in Figure 4(E, F, G). The weight fraction of PS in nanorods/film is obtained at 959 cm^{-1} (in-plane CH wagging of the tetrasubstituted phenylene ring of PPO [62]) and 906 cm^{-1} [23]. Although PPO/PS blends are compatible on the segmental level due to the strong van der Waals interaction between the phenyl ring of PS and the phenylene ring of PPO [63], the similar results in the completely miscible PPO/PS blend nanorods as that in partially miscible PC/PS nanorods are obtained. That is, PS content (Figure 5(B)) in the nanorods of various diameter decreased from position a to position c, a gradient composition distribution was formed along the long axis of nanorods, and PS content in nanorods increased as the rod diameters became smaller.

When compared the PPO/PS blends and PC/PS blends in the nanorods of 300 nm diameter, the PS content at position a in PPO/PS nanorods is less than that in PC/PS nanorods, which also can be observed in position b and c. This trend appeared in the nanorods of 65 and 35 nm diameters as well, showing the PS content in the corresponding PPO/PS blend nanorod is less than that in the PC/PS blend nanorods. This indicates the PS component in the completely miscible blend system is more difficult to enter into nanopores than that in the partially miscible system during the capillary flow. The miscibility of polymer blends also produces significant influence on the composition gradient in nanorods.

4 Nano-TA analysis

The gradient composition distribution in the PC/PS nanorods of 300 nm diameter can be verified by nano-thermal analysis (nano-TA). Nano-TA is a local thermal analysis technique which combines the high spatial resolution imaging capabilities of atomic force microscopy (AFM) with the ability to determine the thermal behaviour of materials with a spatial resolution of sub-100 nm [64, 65]. A special nano-TA probe with embedded miniature heater enables a surface to be visualized with the AFM's routine imaging modes and to target spot of interest to locally investigate the thermal properties of the sample surface, including such thermal transitions as glass transition and melting points. Before measurement, the relationship between the tip temperature and voltage was calibrated by three semicrystalline polymers with known melting temperature: polycaprolactone (333 K), polyethylene (403 K) and polyethylene terephthalate (511 K).

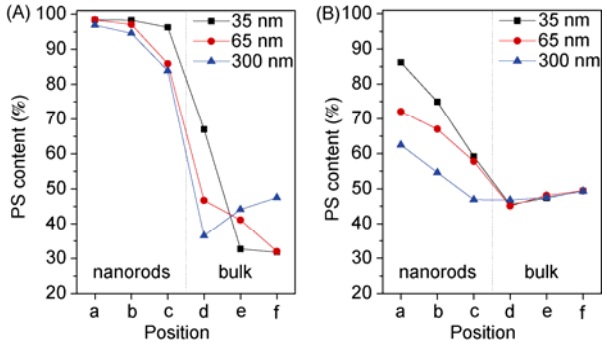

Figure 5 PS content at different positions in nanorods/film of PC/PS blends (A) and PPO/PS blends (B).

To obtain the sample with flat surface suitable for nano-TA measurement, a PC/PS nanorods/film with rod diameter of 300 nm was embedded in a light curable epoxy resin (LCR D-800, TOAGOSEI) and subsequently sectioned using an ultramicrotome. Figure 6(A) shows the topographic images of the sample before indent, obtained in tapping mode under vacuum using a SPI4000 AFM equipped with an Anasys Instruments (AI) nano-TA module and AI nanoscale thermal probes (AN type). The top layer in Figure 6(A) is the PC/PS bulk film, while the bottom aligned array is the nanorod array. Four selected spots (spot 1–4) in the nanorod and bulk film were measured, and after indentation the holes resulting from nano-TA measurements can be clearly observed (Figure 6(B)).

The temperature dependence of the cantilever deflection at different spots is shown in Figure 6(C). During the measurement, the specialized probe is held at a fixed spot on the surface of the sample. As the cantilever and, in turn, the sample heat up at a certain rate (e.g. 5 K/min), the sample expand, pushing the probe up and causing an initial straight rise in the vertical deflection signal. When the temperature reaches the T_g of polymer, the sample will turn soft so that the force applied by the cantilever can deform the surface of sample, allowing the probe to penetrate the sample and decreasing the deflection of the cantilever. Thus, a downward curving is obtained. The point of intersection of the extrapolated upward curving and downward curving is taken as the T_g of amorphous polymer.

In the PC/PS bulk film at spot 4, two transition temperatures are observed at 387.6 K and 427.0 K, which correspond to the T_g of PS-rich regions and PC-rich regions in the blends. At spot 1 in the nanorod array which is far away from the bulk, only one transition can be observed at 392.8 K, which is attributed to the T_g of PS-rich regions. The T_g of PC-rich regions is hard to identify, indicating that the PS content in nanorods is much higher than that in the bulk. At spot 2, the transition temperature of PS-rich regions located at 394.5 K is higher than that at spot 1, revealing the sample at spot 2 contains more high T_g PC composition and thus the PC content at spot 2 is higher than that at spot 1. While at spot 3 which is close to the bulk film, two T_gs, the PS-rich regions at 389.1 K and PC-rich regions at 423.3 K, can be observed. The T_g of PS-rich regions is a little higher than that in the bulk film, while T_g of PC-rich phase is less than that in bulk film, indicating the polymer blends become

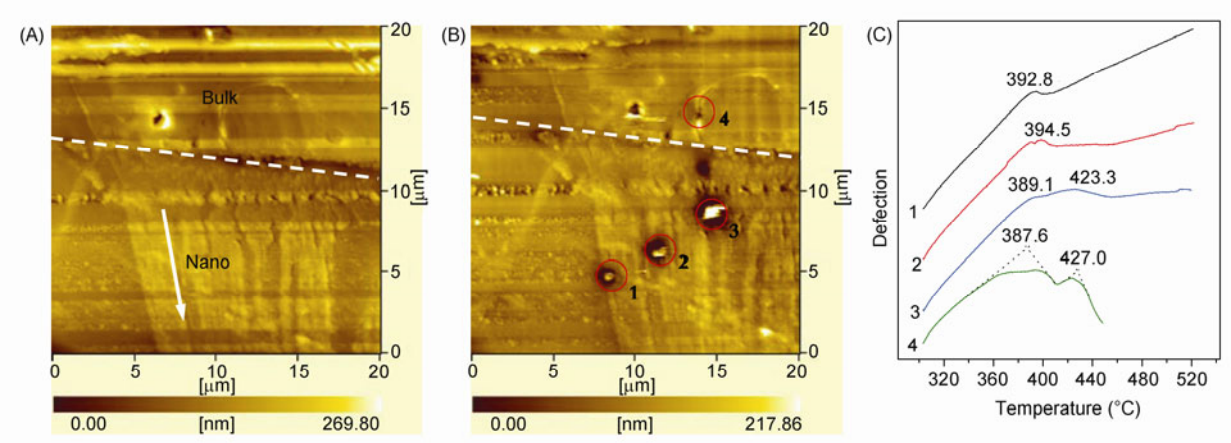

Figure 6 AFM images of PC/PS nanorods/film with rod diameter of 300 nm before (A) and after (B) indent in the nano-TA measurement, (C) temperature dependence of the cantilever deflection in nanorods at spots 1, 2, 3, and in bulk film at spot 4.

more compatible under the nanoconfinement, which accords with results obtained by the scanning force microscopy [66] and linear viscoelastic measurements [67]. The presence of PC-rich regions at spot 3 reveals a higher PC content in the bottom of nanorods. The nano-TA measurements also show that PC content in the bottom of nanorods is higher than that in the top and the compositions in the nanorods are gradient distributed.

5 Composition gradient in nanorods

From the above discussion, gradient composition distribution is formed in nanorods of both partially miscible and completely miscible polymer blends. The schematic illustration of the formation of gradient composition distributed polymer blends in nanorods is shown in Figure 7.

During the polymer blends enter the nanopores by capillary force, several factors which control the composition gradient in nanorods are considered as follows:

(1) Viscosity. For the polymer blend melts to fill up the void space of nanopores, the length of nanorods can be given by Eq. (1) [4, 23, 43]:

$$z = \left(\frac{Rt\gamma \cos\theta}{2\eta} \right)^{1/2} \quad (1)$$

where z is the length of the column of polymer melts in the nanopore, R is the hydraulic radius (the cross-sectional area of a stream divided by the wetted perimeter; R is one half the radius of nanopore), t is the wetting time, γ is the surface tension of the polymer melts, θ is the contact angle at the polymer/capillary wall interface, and η is the viscosity of the polymer melts.

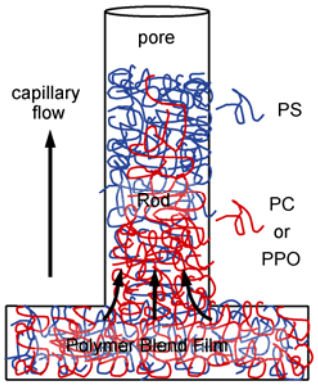

Figure 7 Schematic illustration of the formation of gradient composition distributed polymer blends in nanopores.

In the PC/PS blend melts, the surface tension of PC and PS at 523 K are approximately 25 and 24 mN/m [22]. No profound difference in surface tension can be found between the PC and PS melts. However, the viscosity of PC is up to 8380 (Pa s) [68], while that of PS is only about 170 (Pa s) [69]. For the system of PPO/PS, the melt viscosity of PPO is much higher than PS and the addition of PS can improve the processability of PPO [52]. Therefore, when the blends enter the same nanopores in the same time, it is obvious that the viscosity difference between the polymer melts play a key role to control the length of capillary rise in nanopores. Under the same condition, the compositions with lower viscosity have higher mobility to enter nanopores via the capillary force. Thus, the PS component entered the nanopores more easily than the PC or PPO component and caused a higher content of PS in the nanopores. It is reported that polystyrene of low molecular weights wetted alumina nanopores with much higher rates than that of high molecular weights [21], which is accord with the results that the polystyrene with low viscosity is enriched in nanopores.

For the blend melts within nanopores during the capillary flow, PS component with low viscosity has the higher mobility to keep moving upward, while PC or PPO component with higher viscosity leaves behind and leads to a larger amounts of PC or PPO staying in the bottom of nanorods

(position c), causing that the weight fraction of PC or PPO in the bottom of nanorods is larger than that in the top (position a). Taking into account the polydispersity of the PC and PPO component, it is reasonable to deduce that the content of low molecular weight PC or PPO in nanopores is higher than that in the bulk and a gradient distribution of different molecular weight PC or PPO is also formed in the blend nanorods. As the wetting time increases, the gradient of polymer components in nanopores develops, causing more significant composition difference between the top side and the bottom side of the nanorods. Therefore, during the capillary flow, the difference in viscosity between PS and PC or PPO dominates the formation of gradient composition distribution in polymer blend nanorods.

(2) Miscibility. For the PC/PS bulk melts, due to the partial miscibility of PC/PS [54–56], phase separation occurs [22]. Thus, the phase-separated PS-rich regions contain higher PS content and lower PC content. When starting to anneal the blends/AAO assembly to prepare the blend nanorods, the phase separation in the bulk film and capillary flow of blend melts nanopores took place simultaneously. Therefore, under the driving force of capillary force, the PS-rich regions (less PC component) with lower viscosity preferentially entered into nanopores, while the PC-rich regions was more likely to stay in the bulk film due to its higher viscosity and lower mobility. Whereas for the completely miscible PPO/PS film, due to the strong van der Waals interaction between the phenyl ring of PS and the phenylene ring of PPO [63], the PS component is leashed to enter nanopores by the PPO component. This leads to the fact that the PS in the PPO/PS system has lower rate to enter nanopores than that in the PC/PS system, causing the PS content in the nanorods of completely miscible system is lower than that in the partially miscible system.

(3) Pore diameter. From equation 1, when pore diameters became smaller, the polymer melt required more time to fill the nanopores to get the nanorods with the same length during the capillary flow [4, 23, 43]. Thus, the compositions with higher viscosity, the PC-rich regions in PC/PS blends and the PPO composition in PPO/PS blends, have more difficult time to enter into smaller nanopores owing to the stronger spatial confinement of nanopores. Therefore, under the capillary force, to achieve the highest capillary rise of polymers into nanopores, the smaller nanopores will *select* the polymers with higher mobility to wet the nanopores. Therefore, the PS composition with lower viscosity has more chance to enter into smaller nanopores, leading to the increase of PS content in blend nanorods as the degree of confinement increases.

6 Conclusions

The polymer blend nanorods in various diameters with gradient composition distribution can be prepared by melt-wetting the nanopores with partially miscible PC/PS and completely miscible PPO/PS blend melts. The composition distribution of polymer blends in cylindrical nanopores can be studied by micro-FTIR and nano-TA, which provides a quantitative tool for the analyses of composition gradient of polymer blends in small sections of nanomaterials along the rod direction with satisfactory spatial resolution. When the polymer blends enter into the nanopores by capillary force, the difference of viscosity and miscibility between the polymers, and pore diameter determines the gradient of composition in nanorods. The functional gradient 1-D nanostructured materials may have the novel properties, such as gradient refractive index and gradient mechanical modulus, for the potential application to optical nanodevices, sensor, gecko-tape and biofluidic devices.

This work was supported by a Grant-in-Aid for the Global COE Program "Science for Future Molecular Systems" from the Ministry of Education, Culture, Science, Sports and Technology of Japan. Z.S. thanks the National Natural Science Foundation of China (50921062) for support.

1 Martin CR. Nanomaterials: A membrane-based synthetic approach. *Science*, 1994, 266: 1961–1966
2 Steinhart M. Supramolecular organization of polymeric materials in nanoporous hard templates. *Adv Polym Sci*, 2008, 220: 123–187
3 Shin K, Xiang HQ, Moon SI, Kim T, McCarthy TJ, Russell TP. Curving and frustrating flatland. *Science*, 2004, 306: 76–76
4 Xiang HQ, Shin K, Kim T, Moon SI, McCarthy TJ, Russell TP. Block copolymers under cylindrical confinement. *Macromolecules*, 2004, 37: 5660–5664
5 Sun YM, Steinhart M, Zschech D, Adhikari R, Michler GH, Gösele U. Diameter-dependence of the morphology of PS-b-PMMA nanorods confined within ordered porous alumina templates. *Macromol Rapid Commun*, 2005, 26: 369–375
6 Dobriyal P, Xiang H, Kazuyuki M, Chen J-T, Jinnai H, Russell TP. Cylindrically confined diblock copolymers. *Macromolecules*, 2009, 42: 9082–9088
7 Woo E, Huh J, Jeong YG, Shin K. From homogeneous to heterogeneous nucleation of chain molecules under nanoscopic cylindrical confinement. *Phys Rev Lett*, 2007, 98: 136103
8 Duran H, Steinhart M, Butt HJ, Floudas G. From heterogeneous to homogeneous nucleation of isotactic poly(propylene) confined to nanoporous alumina. *Nano Lett*, 2011, 11: 1671–1675
9 Steinhart M, Göring P, Dernaika H, Prabhukaran M, Gösele U, Hempel E, Thurn-Albrecht T. Coherent kinetic control over crystal orientation in macroscopic ensembles of polymer nanorods and nanotubes. *Phys Rev Lett*, 2006, 97: 027801
10 Wu H, Wang W, Yang H, Su Z. Crystallization and orientation of syndiotactic polystyrene in nanorods. *Macromolecules*, 2007, 40: 4244–4249
11 Steinhart M, Senz S, Wehrspohn RB, Gösele U, Wendorff JH. Curvature-directed crystallization of poly(vinylidene difluoride) in nanotube walls. *Macromolecules*, 2003, 36: 3646–3651
12 Shin K, Woo E, Jeong YG, Kim C, Huh J, Kim KW. Crystalline structures, melting, and crystallization of linear polyethylene in cylindrical nanopores. *Macromolecules*, 2007, 40: 6617–6623
13 Wu H, Wang W, Huang Y, Su Z. Orientation of syndiotactic polystyrene crystallized in cylindrical nanopores. *Macromol Rapid Commun*, 2009, 30: 194–198
14 Wu H, Wang W, Su ZH. Crystallization and orientation of polyethelene in anodic aluminum oxide templates. *Acta Polym Sin*, 2009, 425–429
15 Martin J, Mijangos C, Sanz A, Ezquerra TA, Nogales A. Segmental

dynamics of semicrystalline poly(vinylidene fluoride) nanorods. *Macromolecules*, 2009, 42: 5395–5401
16 Lutkenhaus JL, McEnnis K, Serghei A, Russell TP. Confinement effects on crystallization and curie transitions of poly(vinylidene fluoride-co-trifluoroethylene). *Macromolecules*, 2010, 43: 3844–3850
17 Shin K, Obukhov S, Chen JT, Huh J, Hwang Y, Mok S, Dobriyal P, Thiyagarajan P, Russell TP. Enhanced mobility of confined polymers. *Nat Mater*, 2007, 6: 961–965
18 Martin J, Krutyeva M, Monkenbusch M, Arbe A, Allgaier J, Radulescu A, Falus P, Maiz J, Mijangos C, Colmenero J, Richter D. Direct observation of confined single chain dynamics by neutron scattering. *Phys Rev Lett*, 2010, 104: 197801
19 Serghei A, Chen D, Lee DH, Russell TP. Segmental dynamics of polymers during capillary flow into nanopores. *Soft Matter*, 2010, 6: 1111–1113
20 Wu H, Wang W, Huang Y, Wang C, Su Z. Polymorphic behavior of syndiotactic polystyrene crystallized in cylindrical nanopores. *Macromolecules*, 2008, 41: 7755–7758
21 Zhang MF, Dobriyal P, Chen JT, Russell TP, Olmo J, Merry A. Wetting transition in cylindrical alumina nanopores with polymer melts. *Nano Lett*, 2006, 6: 1075–1079
22 Wu H, Su Z, Takahara A. Molecular composition distribution of polycarbonate/polystyrene blends in cylindrical nanopores. *Polym J*, 2011, 43: 600–605
23 Wu H, Su Z, Takahara A. Gradient composition distribution in poly(2,6-dimethylphenylene oxide)/polystyrene blend nanorods. *Soft Matter*, 2011, 7: 1868–1873
24 Martin J, Mijangos C. Tailored polymer-based nanofibers and nanotubes by means of different infiltration methods into alumina nanopores. *Langmuir*, 2009, 25: 1181–1187
25 Garcia-Gutierrez MC, Linares A, Hernandez JJ, Rueda DR, Ezquerra TA, Poza P, Davies RJ. Confinement-induced one-dimensional ferroelectric polymer arrays. *Nano Lett*, 2010, 10: 1472–1476
26 Chen D, Chen JT, Glogowski E, Emrick T, Russell TP. Thin film instabilities in blends under cylindrical confinement. *Macromol Rapid Commun*, 2009, 30: 377–383
27 Ai SF, Lu G, He Q, Li JB. Highly flexible polyelectrolyte nanotubes. *J Am Chem Soc*, 2003, 125: 11140–11141
28 Azzaroni O, Lau KHA. Layer-by-layer assemblies in nanoporous templates: nano-organized design and applications of soft nanotechnology. *Soft Matter*, 2011, 7: 8709–8724
29 Cepak VM, Martin CR. Preparation of polymeric micro- and nanostructures using a template-based deposition method. *Chem Mater*, 1999, 11: 1363–1367
30 Zheng RK, Chan HLW, Choy CL. A simple template-based hot-press method for the fabrication of metal and polymer nanowires and nanotubes. *Nanotechnology*, 2005, 16: 1928–1934
31 Kimura T, Kobayashi M, Morita M, Takahara A. Preparation of poly(vinylidene fluoride-co-trifluoroethylene) film with a hydrophilic surface by direct surface-initiated atom transfer radical polymerization without pretreatment. *Chem Lett*, 2009, 38: 446–447
32 Quiram DJ, Register RA, Marchand GR, Adamson DH. Chain orientation in block copolymers exhibiting cylindrically confined crystallization. *Macromolecules*, 1998, 31: 4891–4898
33 Huang P, Zhu L, Cheng SZD, Ge Q, Quirk RP, Thomas EL, Lotz B, Hsiao BS, Liu LZ, Yeh FJ. Crystal orientation changes in two-dimensionally confined nanocylinders in a poly(ethylene oxide)-b-polystyrene/polystyrene blend. *Macromolecules*, 2001, 34: 6649–6657
34 Sun L, Zhu L, Ge Q, Quirk RP, Xue CC, Cheng SZD, Hsiao BS, Avila-Orta CA, Sics I, Cantino ME. Comparison of crystallization kinetics in various nanoconfined geometries. *Polymer*, 2004, 45: 2931–2939
35 Huang P, Guo Y, Quirk RP, Ruan JJ, Lotz B, Thomas EL, Hsiao BS, Avila-Orta CA, Sics I, Cheng SZD. Comparison of poly(ethylene oxide) crystal orientations and crystallization behaviors in nano-confined cylinders constructed by a poly(ethylene oxide)-*b*-polystyrene diblock copolymer and a blend of poly(ethylene oxide)-*b*-polystyrene and polystyrene. *Polymer*, 2006, 47: 5457–5466
36 Nojima S, Ohguma Y, Kadena K, Ishizone T, Iwasaki Y, Yamaguchi K. Crystal orientation of poly(ε-caprolactone) homopolymers confined in cylindrical nanodomains. *Macromolecules*, 2010, 43: 3916–3923
37 Chung TM, Wang TC, Ho RM, Sun YS, Ko BT. Polymeric crystallization under nanoscale 2d spatial confinement. *Macromolecules*, 2010, 43: 6237–6240
38 Li D, Xia YN. Electrospinning of nanofibers: Reinventing the wheel? *Adv Mater*, 2004, 16: 1151–1170
39 Liu Y, Cui L, Guan FX, Gao Y, Hedin NE, Zhu L, Fong H. Crystalline morphology and polymorphic phase transitions in electrospun nylon-6 nanofibers. *Macromolecules*, 2007, 40: 6283–6290
40 Zhang CF, Liu YH, Liu SX, Li HZ, Huang K, Pan QH, Hua XH, Hao CW, Ma QF, Lv CY, Li WH, Yang ZL, Zhao Y, Wang DJ, Lai GQ, Jiang JX, Xu YZ, Wu JG. Crystalline behaviors and phase transition during the manufacture of fine denier PA6 fibers. *Sci China Chem*, 2009, 52: 1835–1842
41 Yano T, Yah WO, Yamaguchi H, Terayama Y, Nishihara M, Kobayashi M, Takahara A. Preparation and surface characterization of surface-modified electrospun poly(methyl methacrylate) copolymer nanofibers. *Chem Lett*, 2010, 39: 1110–1111
42 Zhang H, Zhao CG, Zhao YH, Tang GW, Yuan XY. Electrospinning of ultrafine core/shell fibers for biomedical applications. *Sci China Chem*, 2010, 53: 1246–1254
43 Suh KY, Kim YS, Lee HH. Capillary force lithography. *Adv Mater*, 2001, 13: 1386–1389
44 Hu ZJ, Jonas AM. Control of crystal orientation in soft nanostructures by nanoimprint lithography. *Soft Matter*, 2010, 6: 21–28
45 Honda K, Morita M, Masunaga H, Sasaki S, Takata M, Takahara A. Room-temperature nanoimprint lithography for crystalline poly (fluoroalkyl acrylate) thin films. *Soft Matter*, 2010, 6: 870–875
46 He XH, Song M, Liang HJ, Pan CY. Self-assembly of the symmetric diblock copolymer in a confined state: Monte Carlo simulation. *J Chem Phys*, 2001, 114: 10510–10513
47 Li WH, Wickham RA, Garbary RA. Phase diagram for a diblock copolymer melt under cylindrical confinement. *Macromolecules*, 2006, 39: 806–811
48 Zhu YT, Jiang W. Self-assembly of diblock copolymer mixtures in confined states: a Monte Carlo study. *Macromolecules*, 2007, 40: 2872–2881
49 Yu B, Li BH, Jin QH, Ding DT, Shi AC. Confined self-assembly of cylinder-forming diblock copolymers: Effects of confining geometries. *Soft Matter*, 2011, 7: 10227–10240
50 Ma Y, Hu WB, Hobbs J, Reiter G. Understanding crystal orientation in quasi-one-dimensional polymer systems. *Soft Matter*, 2008, 4: 540–543
51 Xiao XQ, Huang YM, Feng JA, Liu HL, Hu Y. Microphase separation of a diblock copolymer dispersed in nanorod arrays grafted on a plate: a Monte Carlo study. *Macromol Theory Simul*, 2011, 20: 124–132
52 Utracki LA. *Polymer Alloys and Blends*. New York: Hanser Publ., 1989
53 Agari Y, Shimada M, Ueda A, Nagai S. Preparation, characterization and properties of gradient polymer blends: discussion of poly(vinyl chloride)/poly(methyl methacrylate) blend films containing a wide compositional gradient phase. *Macromol Chem Phys*, 1996, 197: 2017–2033
54 Patterson D, Robard A. Thermodynamics of polymer compatibility. *Macromolecules*, 1978, 11: 690–695
55 Kim WN, Burns CM. Thermal-behavior, morphology, and the determination of the Flory-Huggins interaction parameter of polycarbonate polystyrene blends. *J Appl Polym Sci*, 1987, 34: 945–967
56 Fekete E, Foldes E, Damsits F, Pukanszky B. Interaction-structure-property relationships in amorphous polymer blends. *Polym Bull*, 2000, 44: 363–370
57 Masuda H, Fukuda K. Ordered metal nanohole arrays made by a two-step replication of honeycomb structures of anodic alumina. *Science*, 1995, 268: 1466–1468

58 Li AP, Muller F, Birner A, Nielsch K, Gösele U. Hexagonal pore arrays with a 50–420 nm interpore distance formed by self-organization in anodic alumina. *J Appl Phys*, 1998, 84: 6023–6026
59 Lee SN, Stolarski V, Letton A, Laane J. Studies of bisphenol-A-polycarbonate aging by Raman difference spectroscopy. *J Mol Struct*, 2000, 521: 19–23
60 Liang CY, Krimm S. Infrared spectra of high polymers. VI. Polystyrene. *J Polym Sci*, 1958, 27: 241–254
61 Kong XM, Xie XM, Yang R, Wang KH, Zhang ZM, Lei H. Determination of the composition distribution of polymer blend films by using microscopic FTIR. *Spectrosc Spect Anal*, 2000, 20: 623–625
62 Nakashima K, Ren Y, Nishioka T, Tsubahara N, Noda I, Ozaki Y. Two-dimensional infrared correlation spectroscopy studies of polymer blends: conformational changes and specific interactions in blends of atactic polystyrene and poly(2,6-dimethyl-1,4-phenylene ether). *J Phys Chem B*, 1999, 103: 6704–6712
63 Wellinghoff ST, Koenig JL, Baer E. Spectroscopic examination of chain conformation and bonding in poly(phenylene oxide)-polystyrene blends. *J Polym Sci, Part B: Polym Phys*, 1977, 15: 1913–1925
64 Yang FZ, Wornyo E, Gall K, King WP. Thermomechanical formation and recovery of nanoindents in a shape memory polymer studied using a heated tip. *Scanning*, 2008, 30: 197–202
65 Maruf SH, Ahn DU, Greenberg AR, Ding Y. Glass transition behaviors of interfacially polymerized polyamide barrier layers on thin film composite membranes via nano-thermal analysis. *Polymer*, 2011, 52: 2643–2649
66 Zhu S, Liu Y, Rafailovich MH, Sokolov J, Gersappe D, Winesett DA, Ade H. Confinement-induced miscibility in polymer blends. *Nature*, 1999, 400: 49–51
67 Liu CY, Zhang BQ, He JS, Keunings R, Bailly C. Confinement effects on chain and glass dynamics in immiscible polymer blends. *Macromolecules*, 2009, 42: 7982–7985
68 Lomellini P. Viscosity-temperature relationships of a polycarbonate melt: williams-landel-ferry versus arrhenius behavior. *Makromol Chem*, 1992, 193: 69–79
69 Fox TG, Flory PJ. The glass temperature and related properties of polystyrene. Influence of molecular weight. *J Polym Sci*, 1954, 14: 315–319